Hindawi
Mathematical Problems in Engineering
Volume 2021, Article ID 9901948, 13 pages
https://doi.org/10.1155/2021/9901948

Research Article

Research on Fuzzy Plastic Constitutive Model Based on Membership Function

Xigang Wang,[1] **Liling Jin**,[1] **and Mingfu Fu**[2]

[1]*School of Resources and Civil Engineering, Liaoning Institute of Science and Technology, Xihu District, Benxi 117004, China*
[2]*School of Civil Engineering and Architecture, Nanchang University, Honggutan District, Nanchang 330031, China*

Correspondence should be addressed to Xigang Wang; fx_wxg@lnist.edu.cn

Received 22 June 2021; Revised 7 October 2021; Accepted 21 October 2021; Published 2 November 2021

Academic Editor: Lei Hou

Soil has no obvious yield point, and the classical elastoplastic theory contradicts the uncertainty of the plastic yield point of the soil. Therefore, a fuzzy plastic Cambridge model based on the membership function was designed by combining the fuzzy mathematics with the Cambridge model. This model made the plastic membership function to correspond with the fuzzy yield function. The plastic strain at any stress state was calculated using the fuzzy Cambridge model and was compared with the indoor triaxial test results, and they were in good agreement. Therefore, it is appropriate to use fuzzy mathematics to express the unobvious soil yield property. The characteristics of soil yield in any stress state is reflected by the fuzzy plastic theory, which indicates that there is entirely no elasticity at any stress state. Moreover, the varying degrees of plasticity and the degree of plastic yield were uniquely determined by the plastic membership function. The fuzzy plastic model used the membership function change to replace the complex hardening. Additionally, the cyclic loading path was clear and appropriate for the cyclic loading and unloading calculations.

1. Introduction

The elastoplastic theory states that the plastic deformation of a material meets a certain yield condition. The elastic and plastic deformations are controlled by the yield condition, and the material's yield point is determined. Numerous experiments have revealed that there is no apparent distinction between the elasticity and plasticity of the soil. Therefore, it is inappropriate to use classic yield conditions to handle the plastic deformation of soil materials, and the effective approach is to use fuzzy mathematics to solve the uncertainty of the soil yield point.

Many engineering structures and components often operate under low cycle fatigue conditions. Cyclic load and cyclic plastic strain are the root causes of material fatigue. Therefore, the problem of cyclic strain analysis of elastic-plastic materials is worth exploring.

The stress point, presented in Figure 1, produced only elastic strain. The plastic strain occurred in accordance with the hardening rule only when the stress point reached the yield line $f(p, q, \varepsilon_v^p) = 0$. The technique to reflect the plastic strain at any point in the elastic region depicted in Figure 1 is a problem that needs to be solved. The stress state within the yield surface did not produce plastic strain to solve this problem Hashiguch [1] proposed a lower load surface concept. Dafalias [2–4] proposed a boundary surface model to calculate the plasticity in the initial yield surface. Klisinski [5] proposed applying fuzzy mathematics to plastic mechanics theory and established the basic framework of fuzzy plastic mechanics. Jiang [6] analyzed the fuzzy factors in elastoplastic mechanics and explained the ambiguity of the yield and failure criterion of concrete materials. Moreover, he proposed the idea of describing the yield state with a membership function. Fu et al. established and demonstrated the uniqueness and existence of the fuzzy elasto-viscoplastic constitutive model along with its solution and studied the continuous transition of elastoplasticity in statics [7, 8]. Wang et al. [9–11] studied the plastic membership function of geotechnical media. They obtained a fuzzy plastic constitutive model suitable for geotechnical media and

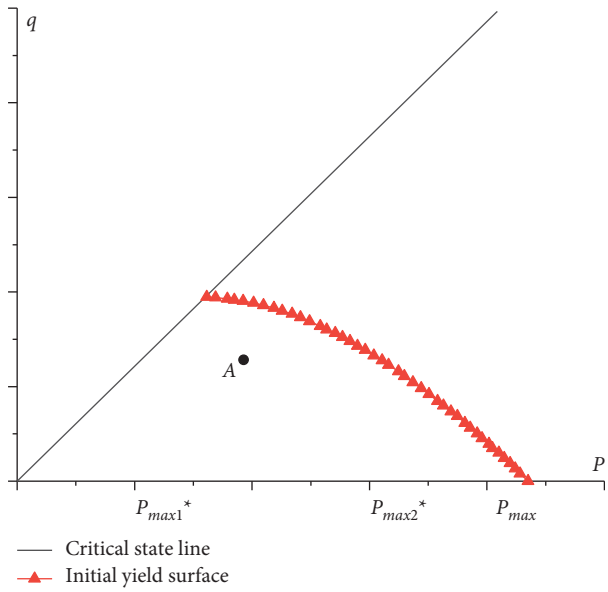

Figure 1: The elastic area of the Cambridge model.

provided a general method for transforming the plastic model into a fuzzy plastic model. Considering the complexity of geotechnical materials, many scholars [12–15] used fuzzy mathematics to analyze geotechnical problems. Landgraf used a multistage load test method to describe the cyclic response of the material. Morrow described the cyclic stress-strain relationship with analytical expressions; however, the expression was not accurate enough to reflect the strength and weakness of the material. Li [16] proposed an improved boundary surface model of remolded clay that considered the elastoplastic loading and unloading processes under cyclic loading. The model adopted a simple boundary surface form, which oversimplified the derivation and calculation of the model theory. Based on the existing constitutive model, Zhao [17] proposed a cyclic boundary surface constitutive model of saturated sand. Zhou [18] proposed a secondary loading surface model suitable for cyclic loading and unloading of rocks based on the Drucker–Prager yield criterion combined with the secondary loading surface. Huang [19] proposed an elastoplastic constitutive model using the boundary surface plasticity theory and described the mechanical properties of unsaturated soil under cyclic loading. Based on the movable hardening criterion of the hardening center and boundary surface, Yao [20] described the anisotropy of soil caused by cyclic loading. Furthermore, he proposed a detailed plastic modulus interpolation method that enabled the model to accurately describe the cyclic stability of saturated clay under low stress levels. Instead of the plastic volumetric strain increment, Dong [21] used hardening parameters independent of the stress path to modify the yield surface of the modified Cambridge model.

The soil yield is unobvious, and the calculation of the cyclic loading and unloading processes is complicated. In this study, we introduce the plastic membership function into the Cambridge model to obtain the fuzzy plastic Cambridge model. The fuzzy plastic Cambridge model is used to describe the fuzziness of the soil yield and solve the problems of cyclic loading and unloading. The fuzzy plastic model uses the change in the fuzzy cone surface to distinctly reflect the loading and unloading paths during cyclic loading and unloading. The continuous change in the plastic membership function can replace the complicated hardening law; therefore, the fuzzy plastic model is more suitable for cyclic loading and unloading problems.

2. Fuzzy Yield Function

2.1. Yield Function Fuzzification. The critical state of the Cambridge model is defined as

$$q = M * p. \tag{1}$$

According to the energy equation and the associated flow law, the plastic potential function of the Cambridge model has the same form as the yield function:

$$f = M \ln p + \frac{q}{p} + C = 0, \tag{2}$$

where C is a constant.

When $q = 0$, the corresponding intersection point of the classical initial yield surface and the p-axis is $p_{\max}$, it can be obtained from equation (2) that $C = -M \ln p_{\max}$, and equation (2) becomes

$$f = M \ln p + \frac{q}{p} - M \ln p_{\max} = 0. \tag{3}$$

According to equation (3), we obtain

$$\ln p_{\max} = \ln p + \frac{1}{M}\frac{q}{p}. \tag{4}$$

The stress points in the elastic region, presented in Figure 1, cannot satisfy equation (4). Moreover, to make the stress points in the elastic region meet the corresponding

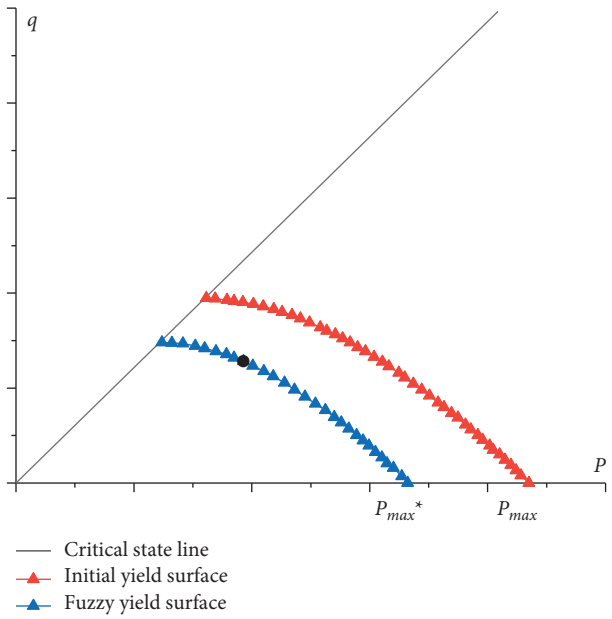

Figure 2: Fuzzy yield surface.

yield function, we need to shift the yield function and $p_{\max}$ to the left at a certain intersection point $p_{\max}^*$. Subsequently, the original stress point in the elastic region is positioned on the corresponding fuzzy yield surface, as shown in Figure 2. Therefore, the fuzzy yield function can be expressed as

$$f^* = M \ln p + \frac{q}{p} - M \ln p_{\max}^* = 0. \quad (5)$$

According to equation (5), when $p_{\max}^*$ moves from right to left, the stress point located in the elastic region (depicted in Figure 1) is positioned on a unique fuzzy yield function f^* based on the stress state.

2.2. Plastic Membership Function. Fuzzy plasticity theory states that the stress state and test parameters determine only the fuzzy yield function established in the classical initial yield function. The stress-state parameter of the fuzzy yield function is $p_{\max}^*$, as shown in Figure 2. Furthermore, as shown in Figure 3, it can also be a combination of stress invariants I_1 and J_2, which represents the size of the hydrostatic pressure axis and deviation on the π plane, respectively. It can also be a combination of other stress or strain invariants. The yield degree (plastic strain) of a fuzzy yield function is determined by the plastic membership function μ that corresponds to the fuzzy yield function and μ is determined by the amount of the stress state that represents f^*.

According to the fuzzy plasticity theory, any stress point in the elastic region depicted in Figure 1 is in a yielding state; however, the degree of yielding varies. There is no absolute elasticity or plasticity in the fuzzy plasticity theory, and it can effectively reflect the elastic region's degree of plasticity in the classical initial yield plane. The fuzzy plastic membership function adopts the assigned plastic membership function form (of course, numerical algorithms such as inversion analysis can be used to determine a more realistic form) to explain the fuzzy plasticity theory. The stress-state parameter adopts $p_{\max}^*$, and the plastic membership function form is

$$\mu = \left(\frac{p_{\max}^*}{p_{\max}}\right)^{\alpha}. \quad (6)$$

In equation (6), α is the model parameter, which can be determined experimentally.

Explanation of fuzzy plastic membership function:

(1) When $\mu = 0$, the fuzzy yield function is the initial yield function of loading, and the yield degree is 0%

(2) When $\mu = 1$, the fuzzy yield function is the classical initial yield function, and the yield degree is 100%

(3) When $0\% < \mu < 100\%$, the fuzzy yield function is between the initial yield function of loading and the classical initial yield function, and the yield degree is $\mu * 100\%$

According to equations (5) and (6), $p_{\max}^*$ determines a plastic membership function value and a fuzzy plastic yield function, and the calculation results of the plastic membership function are presented in Table 1.

The relationship between the different plastic membership function parameters and stress is shown in Figure 4.

As depicted in Table 1 and Figure 4, the corresponding stress and plastic membership function evolution laws are different for different α. When $\alpha < 1$, the plastic membership function and stress exhibited a curved growth relationship; however, the slope kept decreasing. When $\alpha = 1$, the plastic membership function had a linear growth relationship with stress. Furthermore, when $\alpha > 1$, the plastic membership function and stress had a curved growth relationship, and the slope continued to increase. Additionally, with the increase in $p_{\max}^*$, the plastic membership function continuously increased from 0% to 100%, and the degree of plasticity

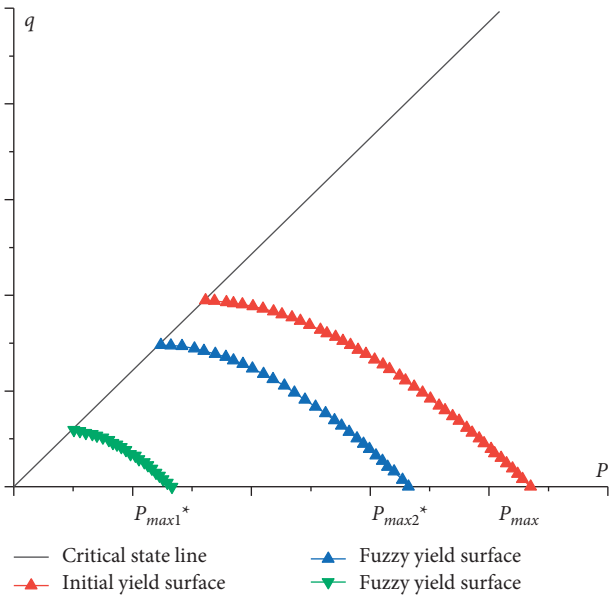

Figure 3: Evolution of fuzzy yield surface.

Table 1: Plastic membership function table.

p_{max}^*	p_{max}	p_{max}^*/p_{max}	$\mu(\%)$ $\alpha = 0.5$	$\alpha = 1$	$\alpha = 2$	$\alpha = 5$	$\alpha = 10$
1.6	188	0.0081	9.21	0.85	0.01	0.00	0.00
10	188	0.0510	23.06	5.32	0.28	0.00	0.00
20	188	0.1020	32.62	10.64	1.13	0.00	0.00
30	188	0.1531	39.95	15.96	2.55	0.01	0.00
40	188	0.2041	46.13	21.28	4.53	0.04	0.00
50	188	0.2551	51.57	26.60	7.07	0.13	0.00
60	188	0.3061	56.49	31.91	10.19	0.33	0.00
70	188	0.3571	61.02	37.23	13.86	0.72	0.01
80	188	0.4082	65.23	42.55	18.11	1.40	0.02
90	188	0.4592	69.19	47.87	22.92	2.51	0.06
100	188	0.5102	72.93	53.19	28.29	4.26	0.18
110	188	0.5612	76.49	58.51	34.23	6.86	0.47
120	188	0.6122	79.89	63.83	40.74	10.60	1.12
130	188	0.6633	83.16	69.15	47.82	15.81	2.50
140	188	0.7143	86.29	74.47	55.45	22.90	5.24
150	188	0.7653	89.32	79.79	63.66	32.33	10.46
160	188	0.8163	92.25	85.11	72.43	44.65	19.94
170	188	0.8673	95.09	90.43	81.77	60.46	36.55
180	188	0.9184	97.85	95.74	91.67	80.46	64.74
185	188	0.9439	99.20	98.40	96.83	92.27	85.14
188	188	1.0000	100.00	100.00	100.00	100.00	100.00

increased from low to high. In the same stress state, the plastic strain and value of α were inversely proportional; the larger the plastic strain, the smaller the value of α, which was determined experimentally.

2.3. Fuzzy Plastic Strain. The fuzzy plastic Cambridge model adopted the associated flow law, and the plastic hardening parameter was the plastic volume strain ε_v^p. The plastic strain increment was orthogonal to the plastic potential surface. The results based on the isotropic consolidation test are shown in Figure 5. The initial void ratio is e_0, and the slopes of the loading and unloading curves are λ and κ, respectively.

The change in void ratio for the load from any point in the elastic region depicted in Figure 1 is

$$\Delta e = e - e_0 = -\lambda \ln \frac{p_{max}^*}{p_0}. \tag{7}$$

The total volumetric strain can be expressed as

$$\varepsilon_v = \frac{-\Delta e}{1 + e_0} = \frac{\lambda}{1 + e_0} \ln \frac{p_{max}^*}{p_0}. \tag{8}$$

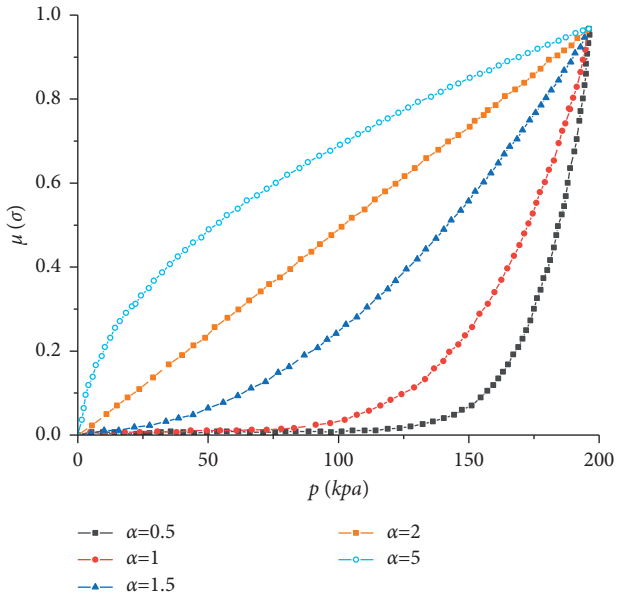

Figure 4: Evolution of plastic membership function.

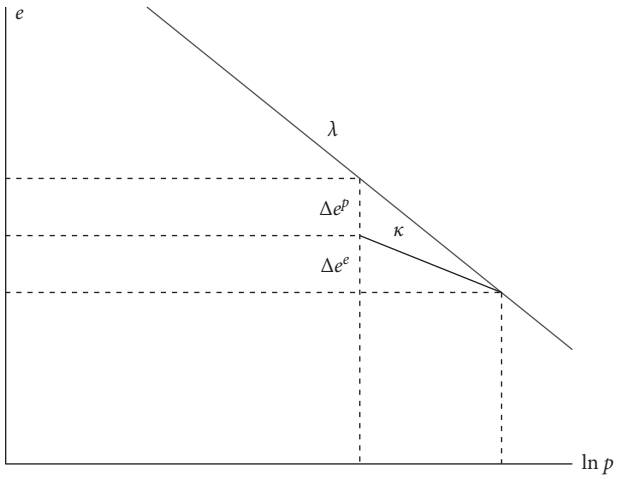

Figure 5: Changes in void ratio.

From equation (8), we can see

$$\varepsilon_v^e = \frac{\kappa}{1+e_0}\left(\ln\ p_{\max}^* - \ln\ p_0\right), \tag{9}$$

$$\varepsilon_v^p = \frac{\lambda-\kappa}{1+e_0}\left(\ln\ p_{\max}^* - \ln\ p_0\right), \tag{10}$$

where ε_v^p is the corresponding plastic volume strain of the fuzzy yield function and f^* is the hardening parameter of the fuzzy plastic Cambridge model.

$$\ln\ p_{\max}^* = \frac{1+e_0}{\lambda-\kappa}\varepsilon_v^p + \ln\ p_0. \tag{11}$$

Substituting equation (11) in (5), we obtain

$$M\ \ln p + \frac{q}{p} - M\left(\frac{1+e_0}{\lambda-\kappa}\varepsilon_v^p + \ln\ p_0\right) = 0. \tag{12}$$

Sorting equation (12), we obtain

$$\frac{\lambda-\kappa}{1+e_0}\ln p + \frac{1}{M}\frac{\lambda-\kappa}{1+e_0}\frac{1}{M}\frac{q}{p} - \varepsilon_v^p - \frac{\lambda-\kappa}{1+e_0}\ln\ p_0 = 0. \tag{13}$$

Let $c_p = \lambda - \kappa/1 + e_0$; then, the fuzzy yield function in equation (12) becomes

$$C_p \ln p + \frac{1}{M}C_p\frac{1}{M}\frac{q}{p} - \varepsilon_v^p - C_p \ln\ p_0 = 0. \tag{14}$$

According to the consistency conditions, we can derive

$$\frac{\partial f^*}{\partial p}\mathrm{d}p + \frac{\partial f^*}{\partial q}\mathrm{d}q + \frac{\partial f^*}{\partial \varepsilon_v^p}\mathrm{d}\varepsilon_v^p = 0. \tag{15}$$

According to equation (14), we know

$$\frac{\partial f^*}{\partial \varepsilon_v^p} = -1. \tag{16}$$

According to the associated flow law, the plastic potential function is orthogonal to the direction of the plastic strain increment, and the fuzzy plastic volume strain can be represented as

$$\mathrm{d}\varepsilon_v^p = \Lambda \frac{\partial g}{\partial p}, \tag{17}$$

where Λ is the plastic scalar factor, which represents the size of the plastic strain increment, and $\partial g/\partial p$ is the development direction of the plastic strain increment. Substituting equations (16) and (17) in (15), we obtain

$$\frac{\partial f^*}{\partial p}\mathrm{d}p + \frac{\partial f^*}{\partial q}\mathrm{d}q - \Lambda^* \frac{\partial g}{\partial p} = 0. \tag{18}$$

According to equation (18), the plastic scalar factor is

$$\Lambda = \frac{(\partial f^*/\partial p)\mathrm{d}p + (\partial f^*/\partial p)\mathrm{d}q}{\partial g/\partial p}. \tag{19}$$

According to the relationship between the plastic potential function and the fuzzy yield function of the Cambridge model, from equation (14), we obtain

$$\frac{\partial f^*}{\partial p} = C_p \frac{1}{p} - C_p \frac{1}{M}\frac{q}{p^2}, \tag{20}$$

$$\frac{\partial f^*}{\partial q} = C_p \frac{1}{M}\frac{1}{p}, \tag{21}$$

$$\frac{\partial g}{\partial p} = \frac{\partial f^*}{\partial p} = C_p \frac{1}{p} - C_p \frac{1}{M}\frac{q}{p^2}. \tag{22}$$

Substituting equations (20)–(22) in (19), Λ can be obtained as

$$\Lambda = \frac{\left[C_p(1/p) - C_p(1/M)\left(q/p^2\right)\right]\mathrm{d}p + \left[C_p(1/M)(1/p)\right]\mathrm{d}q}{C_p(1/p) - C_p(1/M)\left(q/p^2\right)}. \tag{23}$$

Substituting equations (22) and (23) in (17), the plastic strain increment $\mathrm{d}\varepsilon_v^p$ can be obtained as

$$\mathrm{d}\varepsilon_v^p = \left[C_p(1/p) - C_p(1/M)\left(q/p^2\right)\right]\mathrm{d}p + \left[C_p(1/M)(1/p)\right]\mathrm{d}q. \tag{24}$$

According to the Cambridge model equation (22), the relationship between the stress ratio and strain increment is

$$\frac{q}{p} = M - \frac{d\varepsilon_v^p}{d\varepsilon_d^p}, \tag{25}$$

where $\mathrm{d}\varepsilon_d^p$ is the plastic shear strain increment.

Substituting equation (24) in (25), $\mathrm{d}\varepsilon_d^p$ can be obtained as follows:

$$d\varepsilon_d^p = \frac{1}{M - (q/p)}\left[\left[C_p(1/p) - C_p(1/M)\left(q/p^2\right)\right]\mathrm{d}p + \left[C_p(1/M)(1/p)\right]\mathrm{d}q\right]. \tag{26}$$

According to equations (24) and (26), the fuzzy plastic volumetric strain increment $d(\varepsilon_v^p)^*$ and the fuzzy plastic shear strain increment $d(\varepsilon_d^p)^*$ in the elastic region can be obtained as

$$\begin{cases} d\left(\varepsilon_v^p\right)^* = \mu d\varepsilon_v^p = \mu\left[C_p(1/p) - C_p(1/M)\left(q/p^2\right)\right]\mathrm{d}p + \left[C_p(1/M)(1/p)\right]\mathrm{d}q, \\ d\left(\varepsilon_d^p\right)^* = \mu d\varepsilon_d^p = \mu\dfrac{1}{M - (q/p)}\left[\left[C_p(1/p) - C_p(1/M)\left(q/p^2\right)\right]\mathrm{d}p + \left[C_p(1/M)(1/p)\right]\mathrm{d}q\right]. \end{cases} \tag{27}$$

The elastic strain increment was calculated in accordance with elastic theory. After deriving the Cambridge model, the elastic strain increment can be expressed as

$$\begin{cases} \mathrm{d}\varepsilon_v^e = \dfrac{\kappa}{1+e_0}\dfrac{1}{p}\mathrm{d}p, \\ \mathrm{d}\varepsilon_d^e = \dfrac{2}{9}\dfrac{\kappa}{1+e_0}\dfrac{1+\nu}{1-2\nu}\dfrac{1}{p}\mathrm{d}q. \end{cases} \tag{28}$$

The total strain increment was composed of the elastic strain increment $\mathrm{d}\varepsilon^e$ and the fuzzy plastic strain increment $\mathrm{d}(\varepsilon^p)^*$, which can be expressed as

$$\begin{cases} \mathrm{d}\varepsilon_v = \mathrm{d}\varepsilon_v^e + d\left(\varepsilon_v^p\right)^*, \\ \mathrm{d}\varepsilon_d = \mathrm{d}\varepsilon_d^e + d\left(\varepsilon_d^p\right)^*. \end{cases} \tag{29}$$

3. Analysis of Calculation Results

3.1. Model Verification and Parameter Determination. The soil properties of a certain cohesive soil are listed in Table 2. A static triaxial test on the cohesive soil was conducted using a geotechnical triaxial test system, as shown in Figure 6. The cylindrical soil sample had a diameter of 39.1 mm and a height of 80 mm. To ensure the uniformity of the sample, it was compacted in five layers using the wet ramming method. In the triaxial pressure chamber, the soil

Table 2: Cohesive soil parameters.

e_0	ρ (g/cm^3)	ν	E (Gpa)	C (Kpa)	$\phi(^0)$	λ	κ	M
0.65	1.936	0.252	4.565	35	34	0.0865	0.0185	1.33

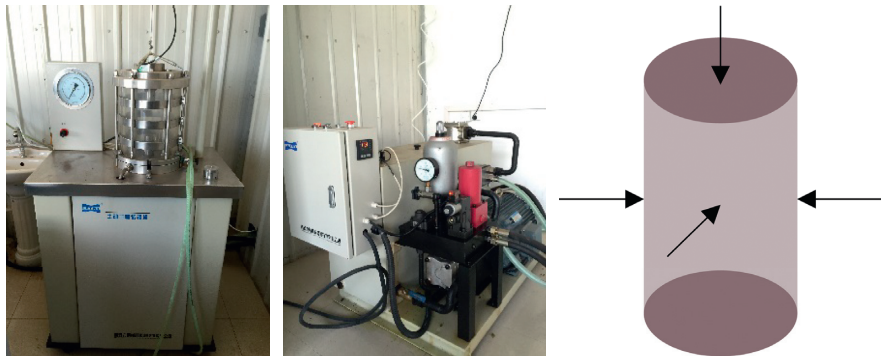

Figure 6: Triaxial test equipment.

sample was saturated by applying back pressure and airless water. The specimens were consolidated under different confining pressures for 24 h in each direction. After consolidation was completed, a static triaxial test was performed under the confining pressures of 30 kPa, 60 kPa, and 90 kPa to verify the reliability of the model.

A comparison between the triaxial test results and the calculation results of the fuzzy plastic Cambridge model is shown in Figure 7.

Figure 7 reveals that the triaxial test results are consistent with the calculation results of the fuzzy plastic Cambridge model. The test result is between $\alpha = 1$ and $\alpha = 1.2$ of the plastic membership function, and when $\alpha = 1.2$, the test result is closer to the calculation result of the fuzzy plastic Cambridge model. The model parameters can be determined by comparing the experiments and models.

3.2. Calculation of the Model. According to equation (22), the loading path values are listed in Table 3.

Modify $p^*_{\max}$ to 188 kPa according to the load path, and when $\alpha = 1$, the calculation results of the fuzzy plastic Cambridge model are presented in Table 4.

The plastic strain results calculated using the fuzzy plastic Cambridge model for varied parameters of the plastic membership function are depicted in Figure 8.

As shown in Figure 8, the plastic strain of the soil material can be easily calculated according to the fuzzy plastic Cambridge model in the original elastic region. When the shear strain and q/p are stable, the larger the plastic membership function parameter, the smaller the plastic body strain. However, when Inp is stable, the larger the plastic membership function parameter, the larger the plastic body strain.

Figure 9 depicts that the plastic body strain and plastic shear strain change continuously with a continuous change in plastic membership function; moreover, the size is controlled by the plastic membership function's value. The greater the value of the plastic membership function, the greater the plastic shear and plastic body strains. Notably, the plastic membership function can effectively reflect the plastic strain of the stress point in the original elastic region, and there is a one-to-one correspondence between the plastic strain and the degree of plastic membership.

3.3. Cyclic Loading and Unloading. Using the soil sample listed in Table 2, the axial cyclic loading and unloading were increased for the test under certain confining pressure conditions. To exhibit the plastic strain inside the initial yield surface, cyclic loading and unloading action were applied between a fuzzy yield surface ($0 < \mu < 1$) and the initial yield surface ($\mu = 1$). The axial dynamic load adopts the form of a sine wave with a frequency of 1 Hz. The law of loading and unloading is defined by

$$q(t) = q_j + q_d * \sin\left(2\pi t + \frac{3}{2}\pi\right), \tag{30}$$

where $q(t)$ represents the magnitude of the dynamic load at time t and q_d represents the dynamic load amplitude.

The initial consolidation pressure of the test soil was 200 kPa, and the values of the cyclic loading are listed in Table 5.

The stress-strain curves calculated using the fuzzy plastic model are shown in Figure 10.

Figure 10 indicates that different initial confining pressures correspond to different plastic membership function values, affecting the cyclic loading and unloading results. When the initial confining pressure is stable, the cyclic loading and unloading curves increase for an increase in the plastic membership function value. Moreover, when the plastic membership function value is stable, the increase in the initial confining pressure increases the cyclic loading and unloading curves. The cyclic loading and unloading path is clear, and its mathematical expression is simple; therefore, fuzzy plasticity theory can solve the problem of cyclic loading and unloading. The loading and unloading path can be noticed using the fuzzy cone surface; thus, the fuzzy plastic theory has more advantages than the classical plastic theory in the cyclic loading and unloading problem.

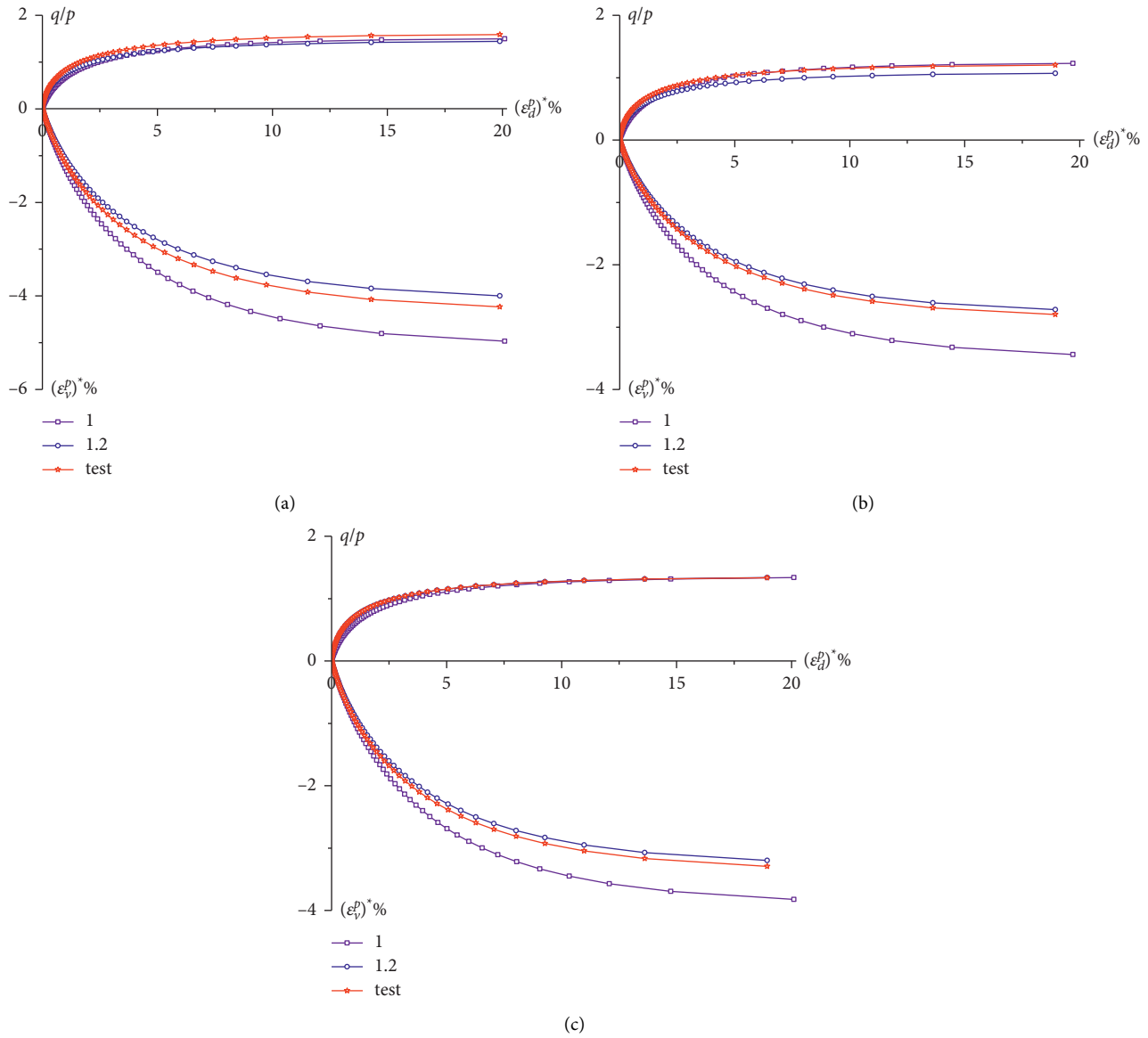

Figure 7: Test comparison curve of $q/p - (\varepsilon_v^p)^* - (\varepsilon_d^p)^*$ for different confining pressures. (a) 30 kpa. (b) 60 kpa. (c) 90 kpa.

Table 3: Load path table.

p	q	$\eta = q/p$	$p_{\max}^*$
1.5942	0.001594191	0.001	1.595390284
2.7742	0.065563384	0.024	2.823927555
3.9542	0.182947243	0.046	4.094166046
5.1342	0.353745768	0.069	5.407175311
6.3142	0.577958959	0.092	6.764049334
7.4942	0.855586815	0.114	8.165907053
8.6742	1.186629338	0.137	9.613892893
9.8542	1.571086526	0.159	11.10917731
11.0342	2.00895838	0.182	12.65295736
12.2142	2.500244901	0.205	14.24645723
13.3942	3.044946087	0.227	15.89092888
14.5742	3.643061938	0.250	17.58765257
15.7542	4.294592456	0.273	19.33793751
16.9342	4.99953764	0.295	21.14312244

Table 3: Continued.

p	q	$\eta = q/p$	$p^*_{\max}$
18.1142	5.757897489	0.318	23.00457629
19.2942	6.569672005	0.340	24.9236988
20.4742	7.434861186	0.363	26.9019212
21.6542	8.353465033	0.386	28.94070684
22.8342	9.325483546	0.408	31.04155191
24.0142	10.35091673	0.431	33.20598609
25.1942	11.42976457	0.454	35.43557332
26.3742	12.56202708	0.476	37.73191248
27.5542	13.74770426	0.499	40.09663813
28.7342	14.9867961	0.522	42.53142129
29.9142	16.27930261	0.544	45.03797019
31.0942	17.62522378	0.567	47.61803106
32.2742	19.02455962	0.589	50.27338894
33.4542	20.47731013	0.612	53.00586846
34.6342	21.9834753	0.635	55.81733475
35.8142	23.54305514	0.657	58.70969419
36.9942	25.15604964	0.680	61.68489538
38.1742	26.82245881	0.703	64.74492995
39.3542	28.54228265	0.725	67.89183351
40.5342	30.31552115	0.748	71.12768653
41.7142	32.14217431	0.771	74.45461534
42.8942	34.02224215	0.793	77.87479303
44.0742	35.95572465	0.816	81.39044046
45.2542	37.94262181	0.838	85.00382727
46.4342	39.98293364	0.861	88.71727286
47.6142	42.07666014	0.884	92.53314749
48.7942	44.2238013	0.906	96.45387327
49.9742	46.42435713	0.929	100.4819253
51.1542	48.67832762	0.952	104.6198328
52.3342	50.98571278	0.974	108.87018
53.5142	53.34651261	0.997	113.2356078
54.6942	55.7607271	1.019	117.7188144
55.8742	58.22835626	1.042	122.3225567
57.0542	60.74940008	1.065	127.0496517
58.2342	63.32385857	1.087	131.9029774
59.4142	65.95173173	1.110	136.8854745
60.5942	68.63301955	1.133	142.0001471
61.7742	71.36772204	1.155	147.2500648
62.9542	74.15583919	1.178	152.6383634
64.1342	76.99737101	1.201	158.1682463
65.3142	79.89231749	1.223	163.8429866
66.4942	82.84067864	1.246	169.6659275
67.6742	85.84245446	1.268	175.6404848
68.5656	88.52504486	1.291	181.0082873
69.0256	89.905844	1.303	183.7912786
69.1500	92.169	1.330	188

Table 4: Calculation results when $\alpha = 1$.

$\eta = q/p$	$p^*_{\max}$	μ	$(\varepsilon_v{}^p)^*$	$(\varepsilon_d{}^p)^*$
0.001	1.595390284	0.008486119	0	0
0.024	2.823927555	0.015020891	−0.000269363	0.000206193
0.046	4.094166046	0.021777479	−0.000547907	0.000423172
0.069	5.407175311	0.028761571	−0.000835868	0.000651513
0.092	6.764049334	0.035978986	−0.001133486	0.000891825
0.114	8.165907053	0.043435676	−0.001441009	0.001144757
0.137	9.613892893	0.051137728	−0.00175869	0.001410999
0.159	11.10917731	0.059091369	−0.002086785	0.001691287
0.182	12.65295736	0.067302965	−0.002425559	0.001986403

Table 4: Continued.

$\eta = q/p$	$p^*_{\max}$	μ	$(\varepsilon_v{}^p)^*$	$(\varepsilon_d{}^p)^*$
0.205	14.24645723	0.075779028	−0.002775281	0.002297185
0.227	15.89092888	0.084526217	−0.003136229	0.002624525
0.250	17.58765257	0.093551343	−0.003508684	0.00296938
0.273	19.33793751	0.10286137	−0.003892934	0.003332772
0.295	21.14312244	0.112463417	−0.004289276	0.003715797
0.318	23.00457629	0.122364767	−0.00469801	0.004119632
0.340	24.9236988	0.132572866	−0.005119446	0.00454554
0.363	26.9019212	0.143095326	−0.005553899	0.004994881
0.386	28.94070684	0.15393993	−0.006001692	0.005469121
0.408	31.04155191	0.165114638	−0.006463155	0.005969839
0.431	33.20598609	0.176627586	−0.006938624	0.006498746
0.454	35.43557332	0.188487092	−0.007428446	0.00705769
0.476	37.73191248	0.200701662	−0.007932972	0.007648678
0.499	40.09663813	0.21327999	−0.008452562	0.008273888
0.522	42.53142129	0.226230964	−0.008987587	0.008935692
0.544	45.03797019	0.239563671	−0.009538421	0.009636677
0.567	47.61803106	0.253287399	−0.010105451	0.010379673
0.589	50.27338894	0.267411643	−0.01068907	0.011167779
0.612	53.00586846	0.281946109	−0.01128968	0.0120044
0.635	55.81733475	0.296900717	−0.011907693	0.012893286
0.657	58.70969419	0.312285607	−0.012543529	0.01383858
0.680	61.68489538	0.328111146	−0.013197618	0.01484487
0.703	64.74492995	0.344387925	−0.013870399	0.015917259
0.725	67.89183351	0.361126774	−0.014562321	0.017061436
0.748	71.12768653	0.378338758	−0.015273843	0.018283772
0.771	74.45461534	0.396035188	−0.016005434	0.01959143
0.793	77.87479303	0.414227622	−0.016757573	0.020992496
0.816	81.39044046	0.432927875	−0.01753075	0.022496147
0.838	85.00382727	0.452148017	−0.018325466	0.024112847
0.861	88.71727286	0.471900388	−0.019142232	0.0258546
0.884	92.53314749	0.492197593	−0.019981571	0.027735261
0.906	96.45387327	0.513052517	−0.020844017	0.029770933
0.929	100.4819253	0.534478326	−0.021730117	0.031980474
0.952	104.6198328	0.556488472	−0.022640428	0.034386158
0.974	108.87018	0.579096702	−0.023575519	0.037014543
0.997	113.2356078	0.602317063	−0.024535975	0.039897639
1.019	117.7188144	0.626163906	−0.025522389	0.043074497
1.042	122.3225567	0.650651897	−0.026535371	0.046593422
1.065	127.0496517	0.67579602	−0.02757554	0.050515137
1.087	131.9029774	0.701611582	−0.028643533	0.054917416
1.110	136.8854745	0.728114226	−0.029739998	0.059902102
1.133	142.0001471	0.755319932	−0.030865597	0.065606152
1.155	147.2500648	0.783245026	−0.032021009	0.072219839
1.178	152.6383634	0.811906188	−0.033206923	0.080018488
1.201	158.1682463	0.841320459	−0.034424048	0.089421975
1.223	163.8429866	0.871505248	−0.035673105	0.101117263
1.246	169.6659275	0.902478338	−0.036954832	0.116345697
1.268	175.6404848	0.934257898	−0.038269982	0.13771866
1.291	181.0082873	0.962810039	−0.039452315	0.168112812
1.303	183.7912786	0.977613184	−0.04006385	0.190350448
1.330	188	1	−0.04124346	0.192589561

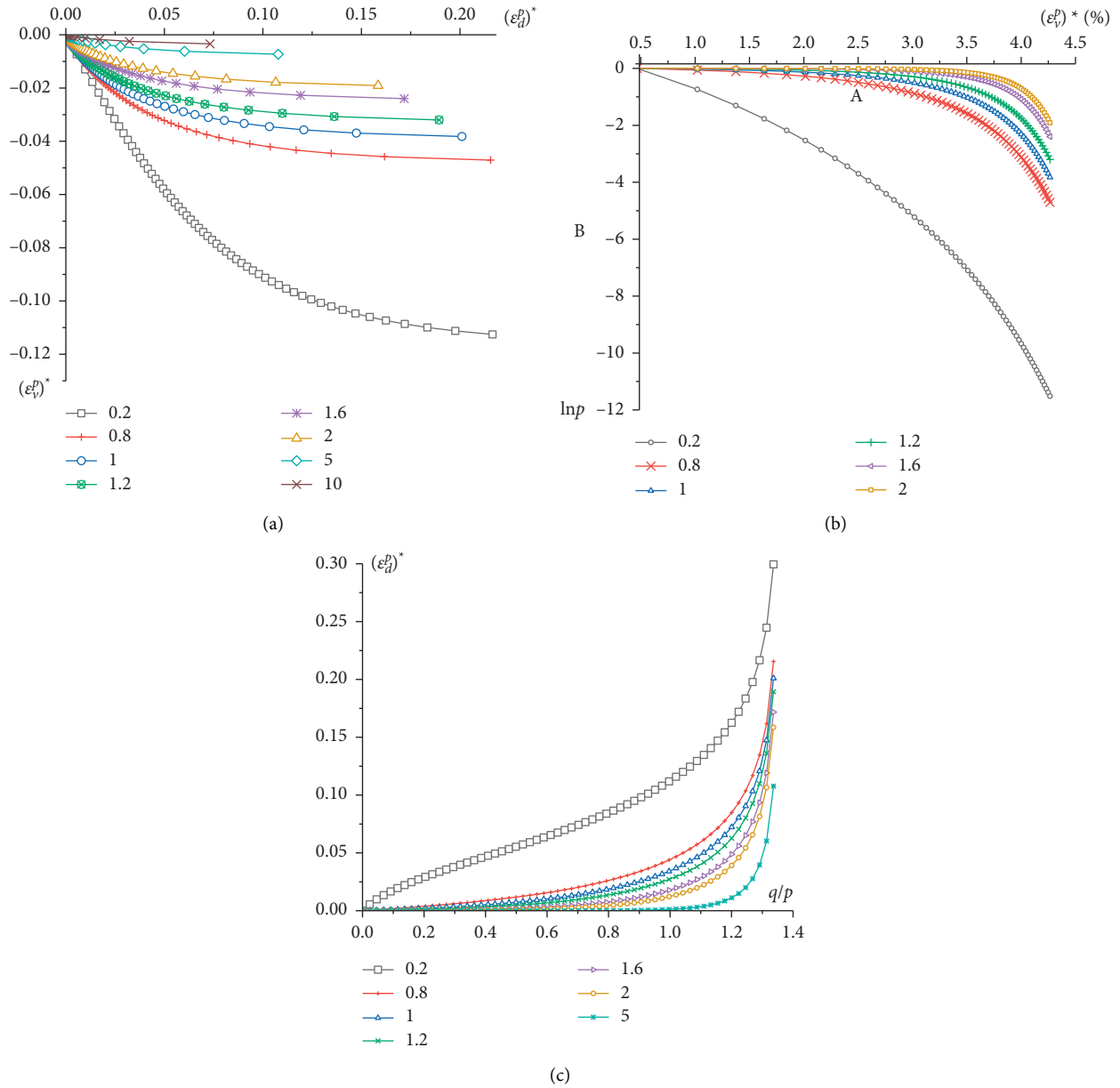

FIGURE 8: The calculation result curve of the fuzzy Cambridge model. (a) Curve of $(\varepsilon_d{}^p)* - (\varepsilon_v{}^p)*$. (b) Curve of $\ln p - (\varepsilon_v^p)^*$. (c) Curve of $q/p - (\varepsilon_d^p)^*$.

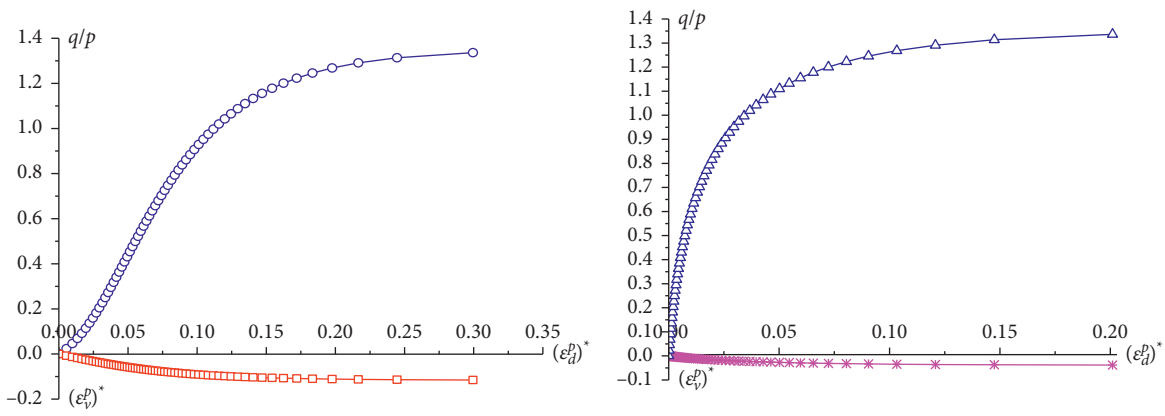

FIGURE 9: Continued.

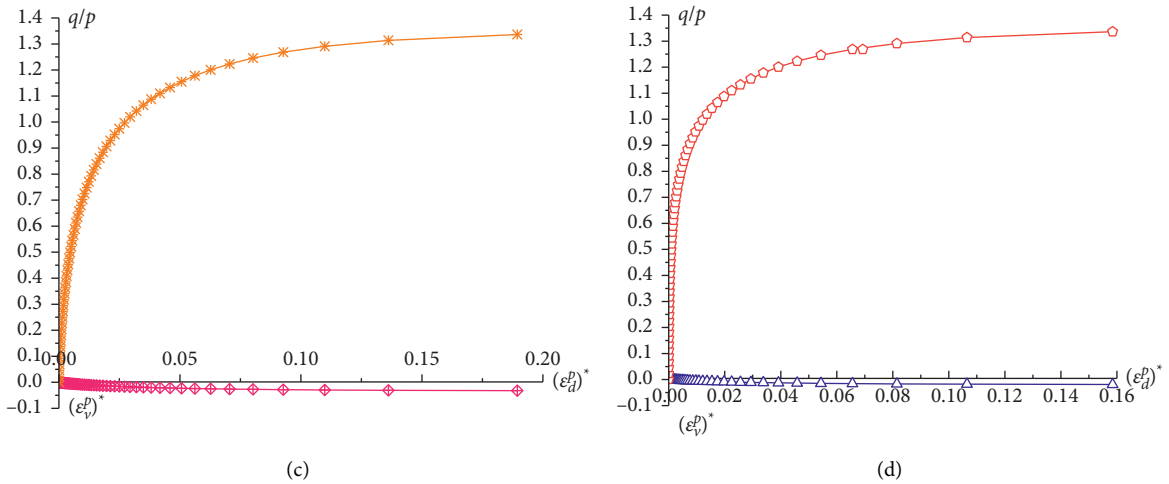

Figure 9: Relationship between plastic membership function and stress-strain. (a) $\alpha = 0.2$. (b) $\alpha = 1$. (c) $\alpha = 1.2$. (d) $\alpha = 2$.

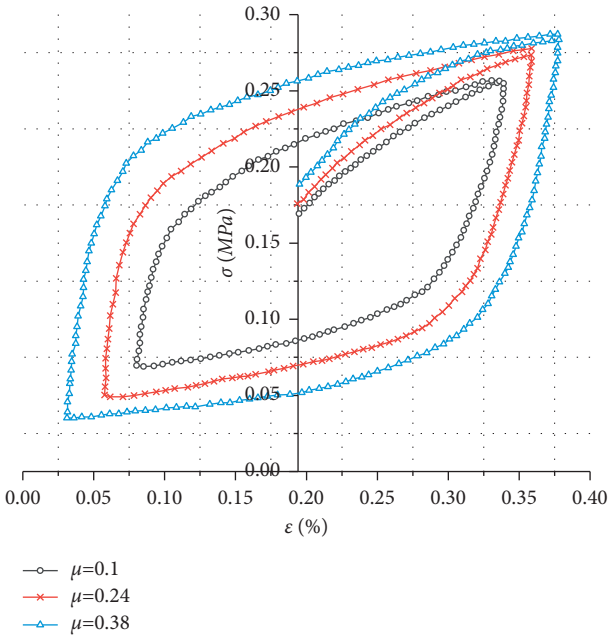

Figure 10: Cycle loading and unloading curves.

Table 5: Cyclic load amplitude values.

p	q_j	q_d	μ	α
90	145	55	0.38	1.2
60	130	70	0.24	1.2
30	115	85	0.10	1.2

4. Discussion

The core of the fuzzy plasticity theory is to select an appropriate plastic membership function. This study adopts the assignment-type plastic membership function form; however, it cannot accurately reflect the plasticity of the material. The subsequent step of the study uses an inversion analysis to determine a more appropriate membership function.

5. Conclusion

This study combined fuzzy mathematics with the Cambridge model and used the associated flow law to obtain a fuzzy plastic Cambridge model. The model reflected the plastic strain of the stress point in the classical initial yield plane and the unobvious characteristics of the soil's yield point. The fuzzy plastic Cambridge model controlled the plastic strain

according to the degree of plastic membership. By comparing and analyzing the fuzzy Cambridge model and the triaxial test results, the model parameters were determined, and the reliability of the fuzzy plastic Cambridge model was verified. The fuzzy plasticity theory considered elastoplasticity. In the cyclic loading and unloading process, the change in the fuzzy cone surface indicated the loading and unloading paths. The mathematical expressions in the loading and unloading processes were simple, and the loading path was clear. This proved that the fuzzy plastic model is appropriate for solving the cyclic loading and unloading problems. The fuzzy plasticity theory is based on fuzzy mathematics and classical plasticity models. Most plastic models can be transformed into fuzzy plastic constitutive models because there is no need to build a new plastic constitutive model. Therefore, fuzzy plasticity theory is easy to popularize.

Data Availability

The data used to support the findings of this study are included within the article.

Conflicts of Interest

The authors declare that they have no conflicts of interest.

Acknowledgments

This research was funded by Liaoning Province Doctor Startup Fund Program by Department of Science and Technology of Liaoning Province (Grant no. 20180540101).

References

[1] K. Hashiguchi, *Elastoplastic Constitutive Laws of Granular Material. Constitutive Equations of Soils*, JSSMFE, Tokyo, Japan, 1977.

[2] Y. F. Dafalias, "Bounding surface plasticity. I: mathematical foundation and hypoplasticity," *Journal of Engineering Mechanics*, vol. 112, no. 9, pp. 966–987, 1986.

[3] Y. F. Dafalias and L. R. Herrmann, "Bounding surface plasticity. II: application to isotropic cohesive soils," *Journal of Engineering Mechanics*, vol. 112, no. 12, pp. 1263–1291, 1986.

[4] A. Anandarajah and Y. F. Dafalias, "Bounding surface plasticity. III: application to anisotropic cohesive soils," *Journal of Engineering Mechanics*, vol. 112, no. 12, pp. 1292–1318, 1986.

[5] M. Klisinski, "Plasticity theory based on fuzzy sets," *Journal of Engineering Mechanics*, vol. 114, no. 4, pp. 563–582, 1988.

[6] S. Jiang and S. Xue, "Analysis of fuzzy factors in elastoplastic mechanics," *Mechanics in Engineering*, vol. 46, no. 4, pp. 37-38, 1989.

[7] M. Fu, B. Xu, and Z. Xiong, "Problem of fuzzy elasto-visco-plasticity and uniqueness and existence of the solution," *Journal of Jiangsu Polytechnic University*, vol. 14, no. 1, pp. 1–11, 1992.

[8] M. Fu, Z. Xiong, and B. Xu, "Analysis of fuzzy elasto-visco-plasticity for spherical shell," *Engineering Mechanics*, vol. 11, no. 2, pp. 1–7, 1994.

[9] X. Wang and M. Fu, "Fuzzy elasto-visco-plasticity analysis of finite deformation based on the L-D plastic flow rule," *Applied Mathematics and Mechanics*, vol. 36, no. 2, pp. 128–139, 2015.

[10] X. Wang, M. Fu, and X. Hu, "Bounding surface model based on membership function under cyclic loading," *Journal of Harbin Engineering University*, vol. 36, no. 12, pp. 1560–1564, 2015.

[11] X. Wang and M. Fu, "Research for constitutive model of fuzzy elastic-plasticity by membership function," *Journal of Vibration and Shock*, vol. 34, no. 23, pp. 115–120, 2015.

[12] X. Shi, Z. Cheng, and L. Wang, "Dentification of geo-material constitutive model using fuzzy system," *Hydro-Science and Engineering*, vol. 33, no. 3, pp. 10–16, 2010.

[13] D. Liu and H. Li, "Application of applied mathematics and fuzzy mathematics in geotechnical engineering," *Chinese Journal of Geotechnical Engineering*, vol. 41, no. 10, p. 1977, 2019.

[14] Z. Fu and T. Liu, "Lope stability analysis based on the renormalization group and fuzzy probability method," *Journal of Transport Science and Engineering*, vol. 31, no. 2, pp. 29–33, 2015.

[15] L. Zhang, E. Chi, M. Zhao, T. Tao, and Y. Li, "Application of fuzzy comprehensive evaluation in rock-soil blasting safety assessment," *Engineering Blasting*, vol. 21, no. 2, pp. 13–17, 2015.

[16] J. Li, S. Chen, and L. Jiang, "An improved bounding surface model for clay under cyclic loading," *Rock and Soil Mechanics*, vol. 36, no. 02, pp. 387–392 + 450, 2015.

[17] C. Zhao, G. Cai, C. Zhao, and W. Zhan, "Cyclic constitutive model of saturated sand based on the bounding surface theory," *Chinese Journal of Solid Mechanics*, vol. 38, no. 3, pp. 244–252, 2017.

[18] Y. Zhou, Q. Sheng, X. Leng, Z. Zhu, and X. Fu, "Preliminary application of subloading surface to cyclic plastic model for rock under cyclic loading," *Chinese Journal of Rock Mechanics and Engineering*, vol. 34, no. 10, pp. 2073–2082, 2015.

[19] M. Huang, C. Yang, and Y. Cui, "Elasto-plastic bounding surface model for unsaturated soils under cyclic loading," *Chinese Journal of Geotechnical Engineering*, vol. 31, no. 6, pp. 817–823, 2009.

[20] H. Yao and J. Wang, "An improved kinematic hardening bounding surface model for saturated clay," *Journal of Tianjin University*, vol. 50, no. 12, pp. 1329–1336, 2017.

[21] X. Dong, C. Zhao, W. Zhang, and C. Zhao, "Cyclic loading boundary surface model of saturated sand based on phase transition state," *Industrial Construction*, vol. 46, no. 07, pp. 129–133+139, 2016.